Boundary-Layer Meteorol (2015) 154:171–187
DOI 10.1007/s10546-014-9970-y

ARTICLE

Revisiting Surface Heat-Flux and Temperature Boundary Conditions in Models of Stably Stratified Boundary-Layer Flows

Jeremy A. Gibbs · Evgeni Fedorovich · Alan Shapiro

Received: 27 March 2014 / Accepted: 21 August 2014 / Published online: 17 September 2014

Abstract Two formulations of the surface thermal boundary condition commonly employed in numerical modelling of atmospheric stably stratified surface-layer flows are evaluated using analytical considerations and observational data from the Cabauw site in the Netherlands. The first condition is stated in terms of the surface heat flux and the second is stated in terms of the vertical potential temperature difference. The similarity relationships used to relate the flux and the difference are based on conventional log-linear expressions for vertical profiles of wind velocity and potential temperature. The heat-flux formulation results in two physically meaningful values for the friction velocity with no obvious criteria available to choose between solutions. Both solutions can be obtained numerically, which casts doubt on discarding one of the solutions as was previously suggested based on stability arguments. This solution ambiguity problem is identified as the key issue of the heat-flux condition formulation. In addition, the agreement between the temperature difference evaluated from similarity solutions and their measurement-derived counterparts from the Cabauw dataset appears to be very poor. Extra caution should be paid to the iterative procedures used in the model algorithms realizing the heat-flux condition as they could often provide only partial solutions for the friction velocity and associated temperature difference. Using temperature difference as the lower boundary condition bypasses the ambiguity problem and provides physically meaningful values of heat flux for a broader range of stability condition in terms of the flux Richardson number. However, the agreement between solutions and observations of the heat flux is again rather poor. In general, there is a great need for practicable similarity relationships capable of treating the vertical turbulent transport of momentum and heat under conditions of strong stratification in the surface layer.

Keywords Boundary conditions · Flux-profile relationships · Monin–Obukhov similarity · Numerical models · Stable boundary layer

J. A. Gibbs (✉) · E. Fedorovich · A. Shapiro
School of Meteorology, University of Oklahoma, 120 David L. Boren Blvd., Suite 5900, Norman, OK 73072, USA
e-mail: gibbz@ou.edu

1 Introduction

In this study we re-examine the surface boundary condition for temperature/buoyancy commonly used in numerical models and simulations of stably stratified atmospheric surface-layer and boundary-layer flows (Garratt 1992; Basu et al. 2008). This condition is typically applied in three possible options. The first applies the condition in terms of potential temperature and kinematic heat flux (also called the potential temperature flux). The second involves virtual potential temperature and virtual potential temperature flux. The final approach relates buoyancy (taken to be proportional to the departure of virtual potential temperature from a prescribed environmental reference value) and kinematic buoyancy flux.

For the sake of brevity we use a version of this condition formulated in terms of potential temperature θ and potential temperature flux Q, with θ_s denoting the potential temperature at a specified level close to the underlying surface and $Q_s = \overline{w'\theta'}_s$ is a near-surface value of the turbulent kinematic heat flux. In the expression for the flux, w' and θ' are, respectively, turbulent deviations of the vertical component w of flow velocity and θ from their corresponding mean values obtained by Reynolds averaging (denoted by the overbar).

In conventional atmospheric modelling, there are two options of implementation of the local temperature boundary condition at the surface. In the *first* option, the heat flux is specified along with values of the mean surface velocity and potential temperature at the first model level above the surface and the aerodynamic roughness length z_0. Then, using integral similarity relationships of the Monin–Obukhov (M–O) theory, the potential temperature value at a specified near-surface level is evaluated. In the *second* option, the potential temperature at a specified near-surface level is known. In this case, one prescribes values of mean velocity and potential temperature at the first model level in combination with specified z_0 and inverts M–O similarity relationships to recover the value of the heat flux. The implementation of these procedures is fraught with certain difficulties, as will be described in the following sections.

2 Boundary Condition Based on Surface Flux

2.1 Implementation of the Flux Condition

In the formulation of the surface flux boundary condition, a local value of the near-surface kinematic heat flux ($Q_s = \overline{w'\theta'}$) is specified. It is either directly prescribed or derived from a land-surface parametrization/model. Also given are the mean wind speed value, U_m, at some model level z_m (located typically a few of metres to a few tens of metres above the ground), mean potential temperature value at the same level (the collocation of the two levels is based on the positioning of these measurements at the Cabauw site whose data are used herein), θ_m, and the value of z_0 where $U_0 = 0$ by definition. Using these parameters, the potential temperature θ_s at some prescribed near-surface level $z_s < z_m$ is evaluated.

Applying the integral M–O similarity relationship for velocity difference $U_m - U_0 = U_m$ along the lines specified in Taylor (1971), Garratt (1992), and Basu et al. (2008), we come to

$$U_m = \frac{u_*}{\kappa}\left(\ln\frac{z_m}{z_0} - \Psi_{u0}\right), \tag{1}$$

where κ is von Kármán's constant (we use its commonly adopted value of 0.4), Ψ_{u0} is the stability correction, which in the general case is a function of z_m/L and z_0/L, u_* is the friction velocity (equal to the square root of the magnitude of the near-surface vertical kinematic momentum flux), and

$$L = -\frac{u_*^3}{\kappa (g/\theta_0) Q_s} \tag{2}$$

is the Obukhov length ($g = 9.81\,\mathrm{m\,s^{-1}}$ is the acceleration due to gravity and θ_0 is a constant reference temperature).

The common choice of expression for Ψ_{u0} in atmospheric surface-layer modelling for stable conditions (Webb 1970; Businger et al. 1971; Hicks 1976), is

$$\Psi_{u0} = -\alpha \frac{z_m - z_0}{L}, \tag{3}$$

with a typical value of the coefficient $\alpha = 5$ (Garratt 1992).

Denoting

$$r_{m0} = \ln (z_m/z_0), \quad \beta = g/\theta_0, \quad \Delta_{m0} = z_m - z_0,$$

and using (2) and (3) Eq. 1 may be rearranged as

$$u_*^3 - u_{*_N} u_*^2 - \frac{\alpha \beta \kappa \Delta_{m0} Q_s}{r_{m0}} = 0, \tag{4}$$

where

$$u_{*_N} = \frac{\kappa U_m}{r_{m0}} \tag{5}$$

may be interpreted as the friction velocity under neutral conditions when the mean velocity follows the logarithmic profile (Basu et al. 2008).

We normalize Eq. 4 by $u_{*_N}^3$ to obtain the following dimensionless cubic equation,

$$\hat{u}_*^3 - \hat{u}_*^2 + Ri_f = 0, \tag{6}$$

where

$$\hat{u}_* = \frac{u_*}{u_{*_N}} \tag{7}$$

is the normalized friction velocity and

$$Ri_f = -\alpha \left(\frac{r_{m0}}{\kappa}\right)^2 \frac{\beta \Delta_{m0} Q_s}{U_m^3}, \tag{8}$$

a quantity proportional to the heat flux, may be interpreted as a modified flux Richardson number. This term represents a dimensionless form of the flux boundary condition and is closely related to the normalized heat flux considered in Basu et al. (2008). A similar representation is employed for the temperature boundary condition (expressed in the form of Ri_B, see Sect. 3.1). Analytical and iterative solutions of Eq. 6 are analyzed in Sect. 2.2.

Next, we obtain the value of $\hat{u}_*$ that corresponds to the maximum Ri_f. Differentiation of Eq. 6 yields

$$\frac{dRi_f}{d\hat{u}_*} = 2\hat{u}_* - 3\hat{u}_*^2. \tag{9}$$

Solving for $\hat{u}_*$ that satisfies $dRi_f/d\hat{u}_* = 0$ gives the trivial solution $\hat{u}_* = 0$ and the non-trivial solution $\hat{u}_* = 2/3 \approx 0.67$. Substituting the latter value into Eq. 6 yields

$$Ri_{f\,\max} = \frac{4}{27} \approx 0.15. \tag{10}$$

Thus, with the employed form of the stability correction function, Eq. 3, there is no physically meaningful solution for the friction velocity in the case $Ri_f > 4/27$, see Fig. 1. Basu et al.

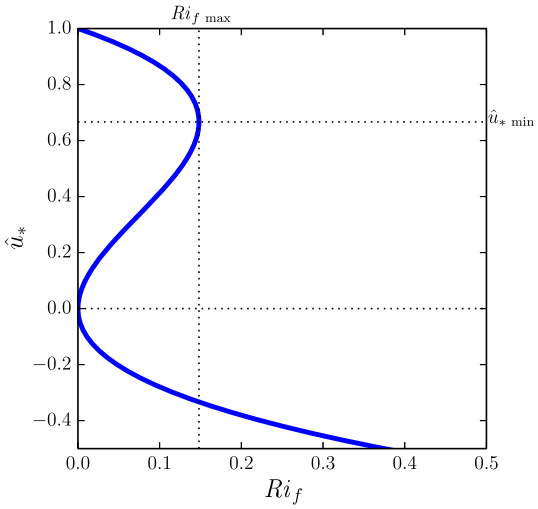

Fig. 1 Dimensionless friction velocity $\hat{u}_*$ as a function of Ri_f after Eq. 6. Negative values indicate that at least one of the Eq. 6 solutions represents non-physical values of u_*

(2008) suggested that $\hat{u}_* = 2/3$ represents the minimum dimensionless friction velocity that can be obtained numerically using the iterative procedure they applied. On the other hand, Basu et al. implied that all roots of (6) that are in the range $0 \leq \hat{u}_* < \hat{u}_{*\min} = 2/3$ are unstable, following the reasoning and terminology of Taylor (1971), and should be discarded. Yet, as will be shown in Sect. 4, these unstable roots are often in reasonable agreement with measured values of friction velocity. Such agreement was previously noted in Wiel et al. (2007).

Once $u_* = \hat{u}_* \kappa U_m / r_{m0}$ is known, the surface-layer (potential) temperature scale is determined from

$$\theta_* = -Q_s / u_* \tag{11}$$

and the M–O flux-profile relationship for the mean potential temperature,

$$\theta_m - \theta_s = \frac{\theta_*}{\kappa} \left[\ln \frac{z_m}{z_s} - \Psi_{\theta s} \right], \tag{12}$$

where the M–O stability correction function for temperature, $\Psi_{\theta s}$, is commonly taken in the form,

$$\Psi_{\theta s} = -\alpha_\theta \frac{z_m - z_s}{L}, \tag{13}$$

with $\alpha_\theta \approx 5$ (Sorbjan 1989), is used to evaluate θ_s as

$$\theta_s = \theta_m + Q_s \frac{r_{ms}}{u_* \kappa} - Q_s^2 \frac{\beta \alpha_\theta \Delta_{ms}}{u_*^4}\ . \tag{14}$$

where

$$r_{ms} = \ln (z_m / z_s) \ \text{ and } \ \Delta_{ms} = z_m - z_s .$$

The value of the temperature difference $\Delta\theta = \theta_m - \theta_s$ can be further used to calculate the bulk Richardson number defined below by (25).

2.2 Solutions of the Cubic Equation for Friction Velocity

2.2.1 Analytical Solution

Following Abramowitz and Stegun (1965) we consider solutions of a general cubic algebraic equation of the form

$$x^3 + a_2 x^2 + a_1 x + a_0 = 0, \tag{15}$$

and define the following supplementary quantities

$$q = \left(\frac{1}{3}\right) a_1 - \left(\frac{1}{9}\right) a_2^2 , \tag{16a}$$

$$r = \left(\frac{1}{6}\right) (a_1 a_2 - 3a_0) - \left(\frac{1}{27}\right) a_2^3 , \tag{16b}$$

$$s_1 = \sqrt[3]{r + \sqrt{q^3 + r^2}} , \tag{16c}$$

$$s_2 = \sqrt[3]{r - \sqrt{q^3 + r^2}} . \tag{16d}$$

The three roots of (15),

$$x_1 = s_1 + s_2 - \frac{a_2}{3} , \tag{17a}$$

$$x_2 = -\frac{s_1 + s_2}{2} - \frac{a_2}{3} + \frac{i\sqrt{3}(s_1 - s_2)}{2} , \tag{17b}$$

$$x_3 = -\frac{s_1 + s_2}{2} - \frac{a_2}{3} - \frac{i\sqrt{3}(s_1 - s_2)}{2}, \tag{17c}$$

have the following properties,
If

(i) $q^3 + r^2 > 0$, one real root and a pair of complex conjugate roots,
(ii) $q^3 + r^2 = 0$, all roots are real and at least two are equal,
(iii) $q^3 + r^2 < 0$, all roots are real.

In addition, the roots satisfy the condition $x_1 x_2 x_3 = -a_0$. Applying this condition in Eq. 6 we find that

$$x_1 x_2 x_3 = -Ri_f . \tag{18}$$

Since Ri_f, as defined in (8), is always positive then in case (i) above Eq. 18 can only be satisfied if the single real root is negative, which is unphysical. In case (iii) above Eq. 18 can only be satisfied if two roots are positive (physical) while the third root is negative (unphysical). We thus conclude that physical (real and non-negative) roots may only be expected if the cubic equation coefficients satisfy the condition $q^3 + r^2 \leq 0$.

Since Eq. 15 becomes Eq. 6 if

$$a_0 = Ri_f , \tag{19a}$$

$$a_1 = 0, \tag{19b}$$

$$a_2 = -1, \tag{19c}$$

the condition $q^3 + r^2 \leq 0$ corresponds to the inequality

$$Ri_f \leq \frac{4}{27}. \tag{20}$$

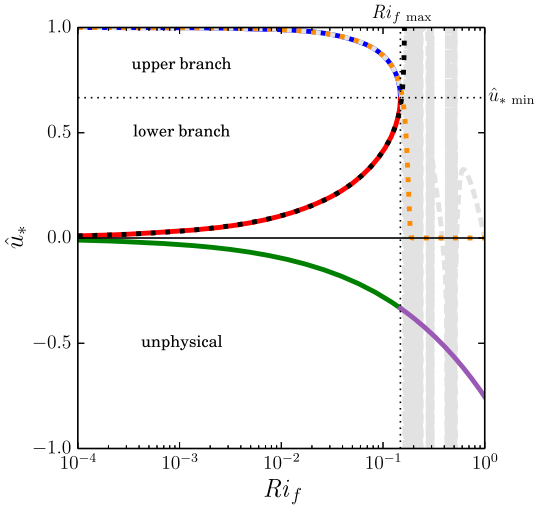

Fig. 2 Analytical and iterative solutions to Eq. 6 as functions of Ri_f. The *blue* and *red* curves correspond, respectively, to the upper-branch and lower-branch real and non-negative (physical) $\hat{u}_*$ roots for $Ri_f \leq Ri_{f\,\max}$. The *green line* shows the negative real (unphysical) $\hat{u}_*$ root branch for $Ri_f \leq Ri_{f\,\max}$. The *purple line* corresponds to the negative real (unphysical) $\hat{u}_*$ root branch for $Ri_f > Ri_{f\,\max}$. The *yellow* and *black dots* show the iterative solutions for $\hat{u}_*$ following Algorithms 1 and 3, respectively. The *grey dashes* merging into gray zones indicate iterative solution by the Algorithm 2. At $Ri_f \leq Ri_{f\,\max}$ this solution is indistinguishable from the upper-branch analytical (*blue line*) and Algorithm 1 (*yellow dots*) solutions

This condition is equivalent to the maximum normalized heat flux identified in Basu et al. (2008). Therefore, Eq. 6 has physical (real and positive) roots, two in total, only if (20) is satisfied. For $Ri_f > Ri_{f\,\max} = 4/27$, the adopted M–O similarity relationship (3) cannot provide usable solutions for u_*. In a slightly different formulation this result was first reported by Taylor (1971) and revisited by Basu et al. (2008).

2.2.2 Iterative Solution

Numerical codes typically solve Eq. 6 iteratively rather than analytically. The iterative algorithm considered in Basu et al. (2008), hereafter called Algorithm 1, is based on a straightforward rearrangement of Eq. 6,

$$\hat{u}_* = \frac{1}{1 + Ri_f/\hat{u}_*^3}\,. \tag{21}$$

To start the iteration procedure, the dimensionless friction velocity corresponding to a neutral flow ($\hat{u}_* = 1$) is substituted into the right-hand side of Eq. 21 to obtain an updated $\hat{u}_*$. The process is repeated for a number of times specified by the user.

The corresponding converged solution for a range of Ri_f is shown in Fig. 2. One can see that with $Ri_f \leq Ri_{f\,\max}$ this solution coincides with the upper branch of the analytical roots ($\hat{u}_* \geq \hat{u}_{*\min} = 2/3$). With $Ri_f > Ri_{f\,\max}$, Algorithm 1 produces $\hat{u}_*$ values dropping practically to zero. From our analytical considerations we know that these values do not represent any solution of the cubic equation (Eq. 6). It is important to note that the failure of Algorithm 1 to produce a legitimate positive solution for $\hat{u}_*$ in this Ri_f range is not a deficiency of the algorithm: such a solution simply does not exist.

We now explore alternative algorithms for the iterative solution of Eq. 6. One possible algorithm (hereafter Algorithm 2) is based on rearranging (6) as

$$\hat{u}_* = 1 - \frac{Ri_f}{\hat{u}_*^2} \,. \tag{22}$$

The procedure again starts with the neutral-flow estimate for $\hat{u}_*$ and continues until convergence. This approach yields the upper-branch analytical root for $Ri_f \leq Ri_{f\max}$, but results in noisy and unstable $\hat{u}_*$ values for $Ri_f > Ri_{f\max}$. However, as discussed above, no physically meaningful solution for $\hat{u}_*$ exists in this range of Ri_f.

Another tested algorithm for iterative solution (Algorithm 3) employs yet another version of Eq. 6,

$$\hat{u}_* = \sqrt{\frac{-Ri_f}{\hat{u}_* - 1}} \,. \tag{23}$$

Initially, $\hat{u}_*$ is set to zero instead of one because this particular formulation does not lead to division by zero. As a result, the converged solution in this case matches the lower-branch analytical root for $Ri_f \leq Ri_{f\max}$.

In this way Algorithms 1 and 3 tie together approximate iterative solutions of Eq. 6 to its full analytical solution for the whole range of acceptable Ri_f that provide $\hat{u}_* \geq 0$.

The duality of the $\hat{u}_*$ solution (when two physical $\hat{u}_*$ roots exist for a single Ri_f proportional to the heat flux Q_s) poses an obvious practical problem because there is no reasonable a priori way to decide which root is preferable. Taylor (1971) conjectured that the first (upper-branch) root is dynamically stable, while the second (lower-branch) root is unstable. This indirectly implied that only the larger of the two physical roots (the upper-branch root in our Fig. 2) should be used. Seeking support for this consideration, Wiel et al. (2007) employed a linear stability analysis to show that the turning point ($\hat{u}_{*\min}$, $Ri_{f\max}$) in the solution separates the stable and unstable roots of Eq. 6. However, as in Basu et al. (2008), only the upper-branch solution for $\hat{u}_*$ was numerically obtained in Wiel et al. (2007), which was used indirectly to imply that for practical purposes only the stable (upper-branch) root should be used. As we have demonstrated above, though, it is entirely possible to iteratively obtain the lower-branch root of Eq. 6 using our Algorithm 3. The usability of this root in model applications is further discussed in Sect. 4.

3 Using Temperature as a Lower Boundary Condition

3.1 Implementation of the Temperature Condition

In the case of the temperature boundary condition, our goal is to calculate the near-surface kinematic heat flux Q_s given values of U_m, θ_m, θ_s, and z_0. By using (14), we obtain

$$\Delta\theta = \theta_m - \theta_s = -Q_s \frac{r_{ms}}{u_* \kappa} + Q_s^2 \frac{\beta \alpha_\theta \Delta_{ms}}{u_*^4} \,. \tag{24}$$

Now we introduce the following bulk Richardson number

$$Ri_B = \frac{\beta \Delta\theta / \Delta_{ms}}{U_m^2 / \Delta_{m0}^2}, \tag{25}$$

which may be related, using (5), (7), (8), and (24) to $\hat{u}_*$ and Ri_f as

$$Ri_B = \frac{\alpha_\theta}{\alpha^2}\frac{Ri_f^2}{\hat{u}_*^4} + \frac{1}{\alpha}\frac{r_{ms}\Delta_{m0}}{r_{m0}\Delta_{ms}}\frac{Ri_f}{\hat{u}_*} . \tag{26}$$

Applying Ri_f obtained from Eq. 6 in Eq. 26 and rearranging the resulting equation yields the following quadratic equation for $\hat{u}_*$ in terms of Ri_B,

$$\hat{u}_*^2 + \frac{F-2G}{G-F}\hat{u}_* + \frac{G-Ri_B}{G-F} = 0, \tag{27}$$

where

$$F = \frac{1}{\alpha}\frac{r_{ms}\Delta_{m0}}{r_{m0}\Delta_{ms}}, G = \frac{\alpha_\theta}{\alpha^2} . \tag{28}$$

Equation 27 is of the form $x^2 + Bx + C = 0$, where

$$B = \frac{F-2G}{G-F}, \quad C = \frac{G-Ri_B}{G-F} . \tag{29}$$

Analytical and iterative solutions for $\hat{u}_*$ are detailed in Sects. 3.2.1 and 3.2.2.

Using (11) and (24), we express $\Delta\theta$ through θ_* and u_*, and obtain with the following quadratic equation for θ_*,

$$\theta_*^2 + \frac{u_*^2}{\alpha_\theta\beta\Delta_{ms}}\frac{r_{ms}}{\kappa}\theta_* - \frac{u_*^2}{\alpha_\theta\beta\Delta_{ms}}\Delta\theta = 0 . \tag{30}$$

We solve this equation analytically (see Sect. 3.2.3) using the value of $\hat{u}_*$ obtained from Eq. 27 and converted to u_* using (6) and (7). After that, we calculate Q_s from (11) and then obtain Ri_f using Eq. 8.

3.2 Solutions for Friction Velocity and Temperature Scale

3.2.1 Analytical Solution of Quadratic Equation for Friction Velocity

Equation 27 has two roots, x_1 and x_2, expressed through $x_{1,2} = -B/2 \pm \sqrt{B^2/4 - C}$. Analysis of the discriminant $B^2/4 - C$, presented in the Appendix, indicates that both roots of Eq. 27 are real under the assumptions $z_m > z_s \geq z_0$ and $\alpha_\theta = \alpha$. Moreover, of the two roots, x_2 (one with the minus in front of the square root) is the only physical root for $Ri_B \leq 1/\alpha$. In the opposite case, when $Ri_B > 1/\alpha$, neither root results in a physical, i.e., belonging to the interval from 0 to 1 (see Appendix), value of $\hat{u}_*$.

Thus, $Ri_{\max} = 1/\alpha$ represents an upper limit of $Ri_{B_{\max}}$ for which a physical $\hat{u}_*$ solution exists within the adopted formulation of the stability-correction function. Since there is only one physical root in this case, using temperature as a lower boundary condition allows us to avoid the duality problem associated with the flux condition. Notably, the temperature condition provides physically relevant $\hat{u}_*$ values also under conditions when $Ri_f > Ri_{f\max}$. This property is illustrated in Fig. 3, where Ri_{B1} corresponding to $Ri_{f\max}$ is indicated together with $Ri_{B\max}$ in relation to the single $\hat{u}_*$ root.

3.2.2 Iterative Solution for Friction Velocity

With a given $\Delta\theta$, the value of the friction velocity in numerical models is commonly obtained using an iterative approach denoted as Algorithm 2 in Basu et al. (2008). We recast it here

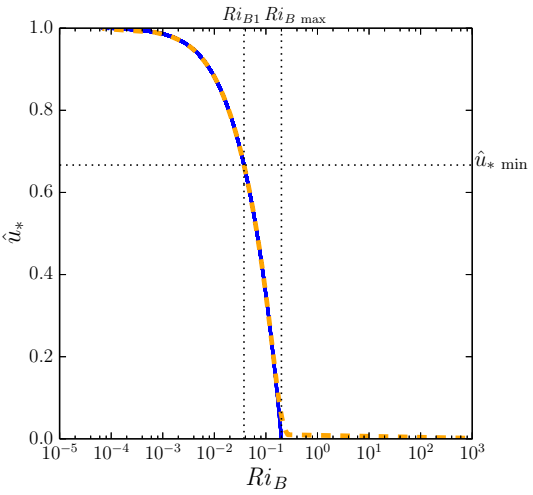

Fig. 3 Analytical and iterative solutions to Eq. 27 as functions of Ri_B. *The blue line* presents the analytical solution. The *yellow dashed line* shows the iterative solution obtained with Algorithm 4

in terms of Ri_f and Ri_B, and refer to it hereafter as Algorithm 4. This algorithm iteratively solves the following sequence of equations,

$$\hat{u}_* = \frac{r_{m0}}{r_{m0} - \Psi_{u0}}, \tag{31a}$$

$$Ri_f = \frac{\alpha r_{m0}}{r_{ms} - \Psi_{\theta s}} \frac{\Delta_{ms}}{\Delta_{m0}} \hat{u}_* Ri_B, \tag{31b}$$

$$L = \alpha \frac{\Delta_{m0}}{r_{m0}} \frac{\hat{u}_*^3}{Ri_f}, \tag{31c}$$

$$\Psi_{u0} = -\alpha \frac{\Delta_{m0}}{L}, \tag{31d}$$

$$\Psi_{\theta s} = -\alpha_\theta \frac{\Delta_{ms}}{L}, \tag{31e}$$

where Ψ_{u0} and $\Psi_{\theta s}$ are set to zero initially and α_θ is taken equal to α. The solution is shown in Fig. 3. For $Ri_B \leq Ri_{B\max}$, the iterative solution closely follows the corresponding analytical solution. Similar to the case of the flux boundary condition, this iterative procedure yields values of $\hat{u}_*$ for Ri_B exceeding $Ri_{B\max}$. Because our analysis of (27) has shown that no physical root of this equation exists beyond $Ri_{B\max}$, any iterative solutions for $Ri_B > Ri_{B\max}$ is spurious.

Basu et al. (2008) also tried to determine the analytical behaviour of u_* as a function of $\Delta\theta$ (in our terms, the dependence of $\hat{u}_*$ on Ri_B). This was accomplished in Basu et al. by first iteratively solving for u_* and Q_s (which would be equivalent to solving for $\hat{u}_*$ and Ri_f) using Eq. 31 and then employing a cubic equation for u_*, a relative of our Eq. 4, to investigate the analytical roots of this equation in relation to stable and unstable, according to Taylor (1971), solutions for u_*. It was found that the u_* solution for $Ri_B \leq Ri_{B1}$ represents the stable solution branch, while the u_* solution for $Ri_B > Ri_{B1}$ represents the unstable solution branch. However, the physical irrelevance of the estimated u_* solutions for $Ri_B > Ri_{B1}$ was not pointed out in Basu et al. (2008). That is to say, it was already shown that there is no solution to Eq. 4 beyond $Ri_{f\max}$. Thus, any discussion of the solution for $Ri_B > Ri_{B1}$ is unwarranted.

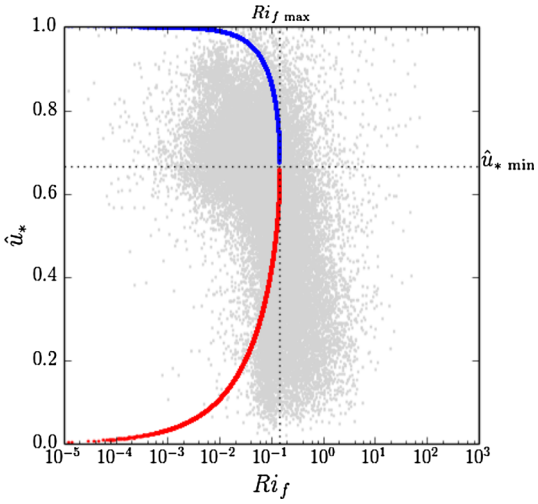

Fig. 4 Normalized friction velocity as a function of observed Ri_f evaluated from Eq. 6 (*blue* and *red dots*) and from Cabauw data (*gray dots*). See Fig. 1 for other notation

3.2.3 Analytical Solution of Quadratic Equation for Temperature Scale

Equation 30 is of the form $x^2 + Bx + C = 0$, with $B = u_*^2 r_{ms} / (\alpha_\theta \beta \kappa \Delta_{ms})$ and $C = -u_*^2 / (\alpha_\theta \beta \Delta_{ms})$. Given the signs of the variables entering expressions for B and C, we conclude that $B > 0$ and $C < 0$, so the discriminant $B^2/4 - C$ is positive, and the roots of the equation are real. We note, however, that only one root $x_1 = -B/2 + \sqrt{B^2/4 - C}$ provides the required positive θ_*.

4 Comparison with Observations

We now explore the applicability of the employed Monin–Obukhov similarity formulations for stable conditions using data from the Cabauw Experimental Site for Atmospheric Research (CESAR; see www.cesar-observatory.nl) for the entire calendar year of 2012. The site collects and records meteorological measurements on wind speed at 10 m, air temperature at 2 and 10 m, and near-surface kinematic heat and momentum fluxes. Turbulent flow statistics (means, variances, and co-variances) are obtained though 10-min averaging. A detailed description of the site's instrumentation is given in Russchenberg et al. (2005).

Cabauw data selected for this study were limited to conditions when the measured $\Delta\theta$ value was positive and the measured Q_s value was negative. While there are occasions when the temperature difference and flux are of opposite sign during stable conditions, the imposed restrictions ensured conditions that M–O relationships are applicable. In terms of notation adopted in the above preceding sections, level z_s was at 2 m, level z_m was at 10 m, and $z_0 = 0.03$ m (Bosveld 2012). In total, 26,350 data points were used in the boundary-condition comparison exercise.

4.1 Evaluation of the Heat-Flux Condition

In Fig. 4, analytical solutions to Eq. 6 are shown as functions of Eq. 8, where the flux Richardson number is calculated using the measured heat flux at the Cabauw tower. Observational values of friction velocity and flux are also shown. As implied by analyses presented in Sect. 2,

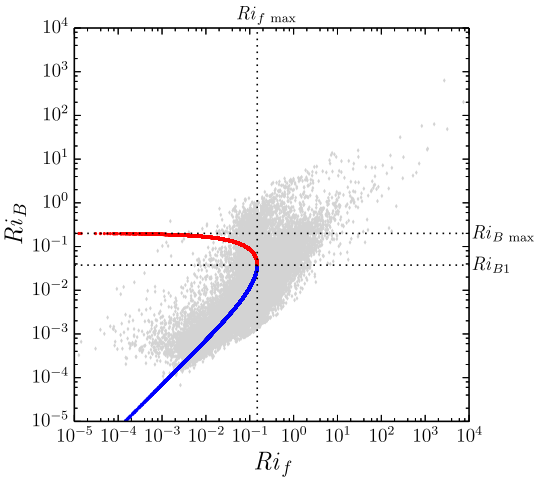

Fig. 5 Calculated (*blue* and *red dots*) and observed (*grey dots*) Ri_B versus observed Ri_f. *Blue* and *red symbols* correspond, respectively, to the upper-branch and lower-branch solutions for $\hat{u}_*$ in Fig. 4. See Figs. 1 and 3 for other notation

there are no analytical solutions for Ri_f exceeding 4/27. Such out-of-limit conditions comprised 9,689 data points, or roughly 37 % of all stably-stratified flow cases considered within the 2012 dataset. Figure 5 relates Ri_f evaluated from the Cabauw data to Ri_B computed based on the flux boundary condition using Eq. 26 and evaluated from the observed $\Delta\theta$ using Eq. 25. For data where $Ri_f < 4/27$, Fig. 5 shows that larger (i.e., upper-branch) solutions for friction velocity produce smaller values of Ri_B (which is merely the normalized temperature difference $\Delta\theta$) and vice versa: the smaller (lower-branch) solutions for u_* produce larger $\Delta\theta$ values. There are 1,698 data points for which the calculated temperature differences obtained with the lower-branch root for u_* were closer to the observed $\Delta\theta$ values than those obtained with the upper-branch root u_*. In other words, if modellers followed the implications of previous studies (Taylor 1971; Wiel et al. 2007; Basu et al. 2008), then 10 % of the considered solutions would yield degraded results.

This appreciable percentage of data, for which values are in better agreement with the lower-branch root than with the upper-branch one, was already noted in Wiel et al. (2007), where the lower branch is termed an unstable branch: "An interesting result is the fact that data points close to the unstable branch are found". It seems unjustified to dismiss the smaller lower-branch root only because of conjecture surrounding physical stability or because it is not readily obtained by a particular iterative algorithm. We have demonstrated above that this lower-branch root is produced by our Algorithm 3. While discussing the suggested rejection of the unstable-branch root in Taylor (1971), Arya (1972) stated that a criterion for choosing between the two roots must come from the observed potential temperature difference $\Delta\theta$ rather than from consideration of the root stability.

Although the Arya (1972) suggestion sounds reasonable, it would be impossible to make any judgment regarding the appropriateness of an individual value of $\Delta\theta$ calculated from the prescribed heat flux value without a priori knowledge of the actual temperature difference. In practice, model simulations would provide two estimates for $\Delta\theta$, although having no information to indicate which of these estimates is more relevant. What is even more discouraging in the analysis of real data based on the considered similarity relationships is the fact that, even if the procedure of selecting the appropriate root were known, the agreement between similarity-theory solutions and experimentally obtained values of u_* and $\Delta\theta$ (expressed in terms of Ri_B) would still be very poor, as evidenced by the measurements shown in Figs. 4 and 5.

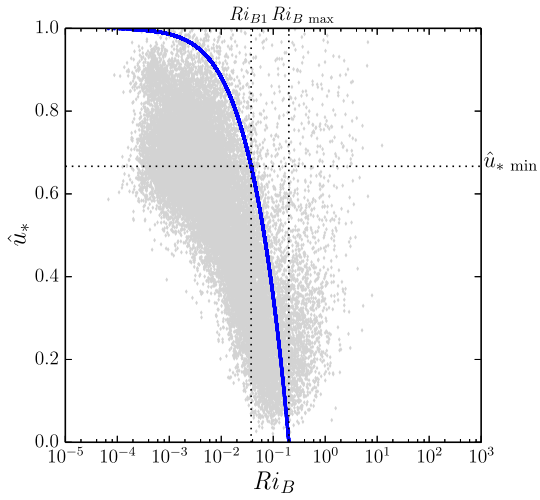

Fig. 6 Normalized friction velocity $\hat{u}_*$ as a function of Ri_B analytically obtained from Eq. 27 (*blue*) and retrieved from Cabauw data (*grey*). See Figs. 1 and 3 for other notation

Specifically, there are 6,126 data points (approximately 37 % of those where $Ri_f \leq 4/27$) in Fig. 4 for which the lower-branch root of u_* is closer to the observed u_* than the upper-branch root. This high percentage of the u_* points that better agree with the lower-branch solution far exceeds the percentage of the $\Delta\theta$ points (10 %) that better fit the lower-branch solution in Fig. 5. Such a disproportion in the amount of relevant data is an indication of a fundamental disconnect between friction-velocity and temperature-difference predictions based on the employed M–O similarity function formulations using the flux boundary condition. Furthermore, the relationship between Ri_f (which is the measure of Q_s) and Ri_B (which is the measure of $\Delta\theta$), experimentally evaluated from the Cabauw data (see Fig. 5), points to the profound failure of the considered similarity expressions to reproduce the observed relationship between these quantities under strong stability conditions (with large Ri_f and Ri_B). It is possible, though, that the latter conditions would be better handled by the recently proposed (Zilitinkevich and Esau 2007) non-linear similarity-function formulations that extend M–O relationships to turbulence regimes with larger Ri_f and Ri_B. These relationships generally predict that the rate of the Ri_f growth with Ri_B gradually decays with increasing stability – a tendency that is only vaguely recognizable in the data presented in Fig. 5.

4.2 Evaluation of the Temperature Condition

In Fig. 6, the analytical solution to Eq. 27 is shown as a function of Ri_B evaluated from the Cabauw data using (25). This figure clearly illustrates the benefit of formulating the lower boundary condition in terms of temperature rather than in terms of heat flux. In the former case, a single value of u_* exists for each value of observed Ri_B satisfying the constraint $Ri_B \leq Ri_{B\max}$ imposed by the employed forms of similarity relationships. In addition to avoiding the duality problem – a crucial disadvantage of the flux condition – the solution for u_* obtained with the temperature condition envelopes observational data over a broader range of stability conditions than in the case of the flux condition (cf. Fig. 4). This previously discussed feature is exhibited by the considerable number of points that fall within the interval between Ri_{B1} and $Ri_{B\max}$. Indeed, in this case there are only 1,570 data points (6 %) that exceed the upper bound of Ri_B, which represents a substantial improvement over the 9,689

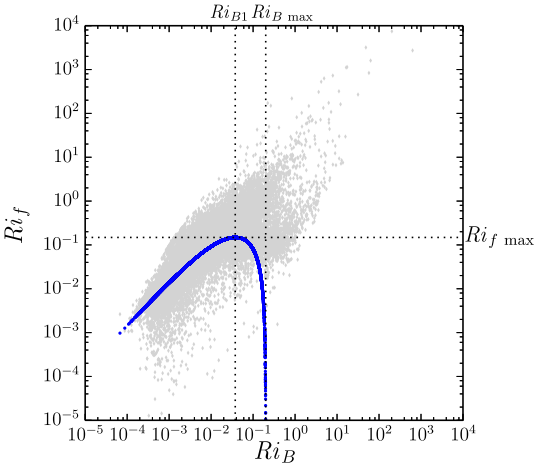

Fig. 7 Calculated (*blue dots*) and observed (*grey dots*) Ri_f versus observed Ri_B. See Figs. 1 and 3 for other notation

outliers (data points spreading beyond $Ri_{f\,\max}$ in Fig. 4) in the case when the flux is used as the lower boundary condition. Another reason in favour of using the temperature-based boundary condition is the relatively large magnitude of potential temperature gradients under stable conditions as compared to turbulent heat fluxes, which are usually small and poorly measurable (Baas et al. 2006).

Despite the advantages of using $\Delta\theta$ as the lower boundary condition in stably-stratified flow models, the agreement between the M–O solutions and observed values of u_* and Q_s (expressed in terms of Ri_f) in Fig. 6 remains marginal. Figure 7 relates Ri_B evaluated from the Cabauw data to Ri_f computed based on the temperature boundary condition and evaluated from the observed Q_s using Eq. 8. Although the solution dualism is not a factor in this case (cf. Fig. 5), we again witness the overall failure of the employed similarity expressions to reproduce the observed relationship between $\Delta\theta$ and Q_s, especially for large values of Ri_B and Ri_f.

5 Summary and Conclusions

Two alternative formulations of the surface thermal boundary condition commonly employed in numerical modelling of atmospheric stably stratified surface-layer flows were evaluated using analytical considerations and observational data from the Cabauw site in the Netherlands. A surface heat-flux formulation and a potential temperature difference formulation were considered. The similarity relationships between the flux and the temperature difference were based on conventional log-linear expressions for the vertical profiles of both wind velocity and potential temperature.

It was confirmed that, in the case of the surface heat-flux formulation, the analytical solution of the problem results in two physically sensible values for the friction velocity u_* (if the solution exists). It was impossible, however, to determine which of these two values was more appropriate (physically relevant) based on available data. The analytical solutions were compared with iterative solutions obtained by three alternative numerical algorithms. It was found that one of the two analytically obtained u_* values, which was identified in previous studies as an unstable root following the terminology of Taylor (1971), was successfully recovered by one of the employed iterative algorithms. This result questions considerations by Wiel et al. (2007) and Basu et al. (2008), whose implication to discard this u_* value

in model applications was, in part, based on the inability of their numerical algorithms to reproduce the unstable, although possibly physically relevant, root.

Comparisons with Cabauw data showed that for approximately 10 % of data points, $\Delta\theta$ values computed using the lower-branch (unstable) root of u_* were closer to the observed values than $\Delta\theta$ values obtained with the upper-branch (stable) root of u_*. This feature suggests that the lower-branch root of u_* should not be dismissed based on the stability arguments, or as a result of the numerical solution inadequacy. Moreover, the agreement between the $\Delta\theta$ values evaluated from similarity solutions and their measurement-derived counterparts from the Cabauw dataset is very poor. In addition, there are 37 % of data points for which the lower-branch (unstable) root of u_* is closer to the observed u_* than the upper-branch root. Therefore, even if a model user could choose the u_* based on a better match of computed $\Delta\theta$ with measurement data, the corresponding computed u_* would not be guaranteed to represent the best match with the observed u_*.

It was demonstrated that using temperature as the lower boundary condition eliminates the duality issue and provides physically sensible values of heat flux for a broader range of stability condition in terms of the flux Richardson number Ri_f. While this approach does not require one to choose between two roots of u_*, the agreement between solutions and observations of Q_s remains poor overall. The limitations of the employed similarity expressions are particularly evident in strongly stable regimes, when the observed relationship between Q_s and $\Delta\theta$ (in terms of Ri_f versus Ri_B) strongly deviates from the behaviour predicted by the considered similarity relationships. Physically, this behaviour represents a scenario where the increasing temperature gradient progressively inhibits the turbulent heat flux but does not completely reduce it to zero as implied by the considered similarity relationships.

Our study thus provides further arguments in favour of using a temperature surface condition in models of stably stratified boundary-layer flows based on log-linear flux-profile M–O similarity relationships in the surface layer. The application of the heat-flux condition in this case is fraught with duality of solutions and is limited to a narrower stability range compared to the temperature condition. Extra caution should be paid to the iterative procedures used in the heat-flux condition calculations as they often provide only partial solutions for the friction velocity and associated temperature difference.

In general, the need is evident for practicable similarity relationships capable of treating the turbulent transport of momentum and heat under conditions of strong stratification in the surface layer. The applicability of the similarity relationships proposed in Zilitinkevich and Esau (2007)) for formulating the thermal boundary conditions should be investigated in this regard. Without such new relationships being verified and implemented, the conventional iterative algorithms employed for imposing thermal surface boundary conditions in boundary-layer models will continue to produce irrelevant values of u_*, $\Delta\theta$, and Q_s, and the performance of the near-surface flux-profile parametrizations in strongly stable boundary-layer flows will remain largely inadequate.

Acknowledgments We acknowledge the Royal Netherlands Meteorological Institute (KNMI) and F. Bosveld (KNMI) for making the Cabauw data available.

Appendix

By evaluating the discriminant $B^2/4 - C$ in Sect. 3.2.1 one can assess whether the roots of Eq. 27 are real or complex. The condition for solutions to be real is $B^2/4 \geq C$. Invoking (29) for B and C, this condition provides

$$Ri_B(G - F) \geq -F^2/4. \tag{32}$$

We now show that $G - F$ on the left-hand side of Eq. 32 is non-negative. First use (28) to write $G - F$ as

$$G - F = \frac{\alpha_\theta}{\alpha^2} - \frac{1}{\alpha}\frac{r_{ms}\Delta_{m0}}{r_{m0}\Delta_{ms}}. \tag{33}$$

In view of the definitions of β, r_{m0}, r_{ms}, z_0, and z_s, we obtain

$$\begin{aligned}\frac{r_{ms}\Delta_{m0}}{r_{m0}\Delta_{ms}} &= \frac{\ln(z_m/z_s)}{\ln(z_m/z_0)}\frac{(z_m - z_0)}{(z_m - z_s)} \\ &= \frac{\ln\left[1 - (1-\gamma)\right]}{1-\gamma}\frac{1-\mu}{\ln\left[1-(1-\mu)\right]},\end{aligned}$$

where $\gamma = z_s/z_m$ and $\mu = z_0/z_m$. The Taylor series expansion,

$$\ln(1-x) = -\left(x + \frac{x^2}{2} + \frac{x^3}{3} + \frac{x^4}{4}\ldots\right),$$

with $1-\gamma$ and $1-\mu$ used in place of x, yields

$$\frac{r_{ms}\Delta_{m0}}{r_{m0}\Delta_{ms}} = \frac{1 + \frac{(1-\gamma)}{2} + \frac{(1-\gamma)^2}{3} + \frac{(1-\gamma)^3}{4} + \cdots}{1 + \frac{(1-\mu)}{2} + \frac{(1-\mu)^2}{3} + \frac{(1-\mu)^3}{4} + \cdots}.$$

Under the natural assumption of $z_m > z_s \geq z_0$, we have $\gamma \geq \mu \geq 0$, and therefore $r_{ms}\Delta_{m0}/(r_{m0}\Delta_{ms}) \leq 1$. Further assuming (as done in most model applications) $\alpha_\theta = \alpha$, we conclude that $G - F$ is non-negative and thus the right-hand side of Eq. 32 is non-positive. On the other hand, Ri_B is non-negative under stable/neutral conditions for which (32) is satisfied, and thus Eq. 27 is guaranteed to have two real roots.

Next we must determine whether these roots are physically meaningful. First we note that the dimensionless friction velocity must be greater than zero. Combining the definitions of β, r_{m0}, r_{ms}, z_0, and z_s with (1), (5), and (7), we obtain

$$\hat{u}_* = \frac{r_{m0}}{r_{m0} - \Psi_{u0}}. \tag{34}$$

Noting that Ψ_{u0} is negative (see Eq. 3), we conclude that $\hat{u}_*$ must also be less than unity. Thus, the roots of Eq. 27 must satisfy $0 < \hat{u}_* < 1$.

We also need to determine ranges of variability of B and C (Eq. 29). Taking into account that $G - F$ is non-negative and $\alpha_\theta = \alpha$, the difference

$$F - 2G = \frac{1}{\alpha}\left(\frac{r_{ms}\Delta_{m0}}{r_{m0}\Delta_{ms}} - 2\right) \tag{35}$$

is negative since $r_{ms}\Delta_{m0}/(r_{m0}\Delta_{ms}) \leq 1$ (see above), it becomes clear that B is always negative. Considering the numerator of C,

$$G - Ri_B = \frac{1}{\alpha} - Ri_B, \tag{36}$$

we find that

$$C \geq 0 \quad \text{if } Ri_B \leq 1/\alpha, \tag{37a}$$

$$C < 0 \quad \text{if } Ri_B > 1/\alpha. \tag{37b}$$

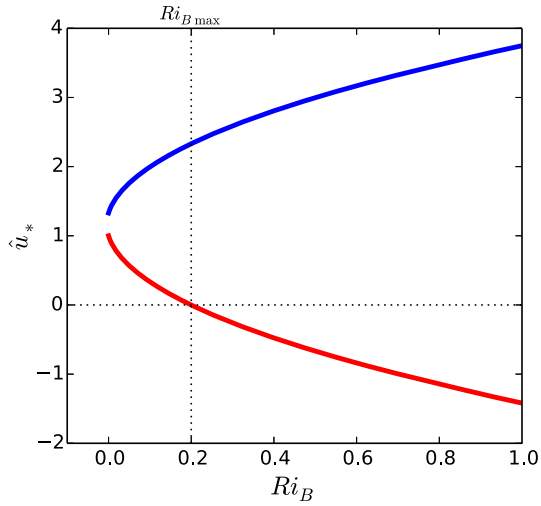

Fig. 8 Roots of Eq. 27 as functions of Ri_B. The *blue line* indicates the x_1 root (note that its value at $Ri_B = 0$ is equal to $-B$), and the *red line* indicates the x_2 root

Now consider

$$x_1 = -\frac{B}{2} + \sqrt{\frac{B^2}{4} - C},\ x_2 = -\frac{B}{2} - \sqrt{\frac{B^2}{4} - C}\,. \tag{38}$$

Because the condition $B^2/4 \geq C$ is globally satisfied and B is non-negative, $x_1 > 0$ regardless of whether C is positive or negative. On the other hand, $x_2 < 0$ when $C < 0$, and $x_2 > 0$ when $C > 0$.

However, as previously noted, we need $\hat{u}_* < 1$, so the following condition:

$$x_1 = -\frac{B}{2} + \sqrt{\frac{B^2}{4} - C} < 1$$

must be satisfied for x_1. According to (28) and (29), this would require $Ri_B < 0$, so x_1 is physically irrelevant. Conversely, with $C > 0$ and $Ri_B < 1/\alpha$, see (37), we come to $0 < x_2 < 1$, so in this case x_2 is a physically relevant root.

Collecting results, we see that there is no physical solution for $\hat{u}_*$ when $Ri_B > 1/\alpha$. When $Ri_B \leq 1/\alpha$, Eq. 27 provides only one physical root given by $-B/2 - \sqrt{B^2/4 - C}$. Thus, $1/\alpha = 0.2$ is the maximum value of Ri_B for which a physically relevant $\hat{u}_*$ exists within the framework of the adopted assumptions. This solution behaviour is illustrated in Fig. 8.

References

Abramowitz M, Stegun IA (1965) Handbook of mathematical functions with formulas, graphs, and mathematical tables. Dover, New York 1046 pp

Arya SPS (1972) Comment on the paper by P. A. Taylor: 'A note on the log-linear velocity profile in stable conditions'. Q J R Meteorol Soc 98:460–461

Baas P, Steeneveld GJ, van de Wiel BJH, Holtslag AAM (2006) Exploring self-correlation in fluxgradient relationships for stably stratified conditions. J Atmos Sci 63:3045–3054

Basu S, Moene AF, Holtslag AAM, Steeneveld G-J, van de Wiel BJH (2008) An inconvenient "truth" about using sensible heat flux as a surface boundary condition in models under stably stratified regimes. Acta Geophys 56(1):88–99

Bosveld FC (2012) Cabauw observational program on landsurface-atmosphere interaction (2000-today). Online at http://www.knmi.nl/bosveld/experiments/documentation. Accessed 18 Feb 2014
Businger JA, Wyngaard JC, Izumi Y, Bradley EF (1971) Flux-profile relationships in the atmospheric surface layer. J Atmos Sci 28:181–189
Garratt JR (1992) The atmospheric boundary layer. Cambridge University Press, Cambridge 316 pp
Hicks BB (1976) Wind profile relationships from the Wangara experiment. Q J R Meteorol Soc 102:535–551
Russchenberg H, Bosveld F, Swart D, ten Brink H, de Leeuw G, Uijlenhoet R, Arbesser-Rastburg B, van der Marel H, Ligthart LP, Boers R, Apituley A (2005) Ground-based atmospheric remote sensing in the Netherlands: European outlook. IEICE Trans Commun 88-B(6):2252–2258
Sorbjan Z (1989) Structure of the atmospheric boundary layer. Prentice Hall, New Jersey 317 pp
Taylor PA (1971) A note on the log-linear velocity profile in stable conditions. Q J R Meteorol Soc 97:326–329
van de Wiel BJH, Moene AF, Steeneveld G-J, Hartogensis OK, Holtslag AAM (2007) Predicting the collapse of turbulence in stably stratified boundary layers. Flow Turbul Combust 79(3):251–274
Webb EK (1970) Profile relationships: the log-linear range, and extension to strong stability. Q J R Meteorol Soc 96:67–90
Zilitinkevich S, Esau I (2007) Similarity theory and calculation of turbulent fluxes at the surface for the stably stratified atmospheric boundary layer. In: Baklanov A, Grisogono B (eds) Atmospheric boundary layers. Springer, New York, pp 37–49